Combinatorial Mapping of the Phase Behavior of ABC Triblock Terpolymers in Thin Films: Experiments

S. Ludwigs,*,† K. Schmidt,† C. M. Stafford,‡ E. J. Amis,‡ M. J. Fasolka,‡ A. Karim,‡ R. Magerle,† and G. Krausch*,†,§

Physikalische Chemie II and Bayreuther Zentrum für Kolloide und Grenzflächen (BZKG), Universität Bayreuth, D-95440 Bayreuth, Germany and Polymers Division, National Institute of Standards and Technology (NIST), Gaithersburg, Maryland 20899

Received May 14, 2004; Revised Manuscript Received September 7, 2004

ABSTRACT: We report on the thin film phase behavior of poly(styrene)-*block*-poly(2-vinylpyridine)-*block*-poly(*tert*-butyl methacrylate) triblock terpolymers with volume fractions ϕ_{PS}:ϕ_{P2VP}:ϕ_{PtBMA} scaling as 1:1.2:*x*, with *x* ranging from 3.05 to 4. On controlled annealing in the vapor of a nearly nonselective solvent the films form terraces of well-defined thickness with a highly ordered hexagonally perforated lamella structure. Using a gradient combinatorial technique we are able to systematically map the dependence of the morphology on the film thickness. By use of substrates with different surface energy we demonstrate that the perforated lamella is a stable phase, regardless of the chemical nature of the substrate, which makes the structure and methodology robust for application in nanotechnology.

Introduction

In recent years block copolymers[1−3] have attracted increasing interest as a promising means to create nanopatterned surfaces[4−7] since they self-assemble into highly ordered structures with characteristic domain spacings between 5 and 50 nm (for a review, see ref 7). Recent developments in controlled synthesis[8−11] together with theoretical models[12−23] allow one to precisely control the morphology and length scale of the microdomains. In particular, ABC triblock terpolymers form a large variety of well-ordered microdomain structures of molecular dimension.[2,24,25] Introduction of functional components and subsequent chemical modification may lead to properties tailored for specific applications.

While block copolymer melts and block copolymer solutions usually show a rather random distribution of microdomain orientations in the bulk, additional driving forces for the structure formation exist near surfaces and in thin films.[26−28] Typically the polymeric component with the lowest surface energy preferentially accumulates at the surface and the component with the lowest interfacial energy is attracted to the supporting substrate. The presence of such external surfaces and confinement of the material to a film thickness comparable to the bulk domain spacing can result in large-scale alignment of the microdomains and stabilization of novel domain structures, which have been recently identified as surface reconstructions.[29−36]

The majority of studies on block copolymer nanolithography has focused on thin films of diblock copolymers, which exhibit spheres or cylinders of the minority component. When the surfaces preferentially attract the majority block, the cylinders align parallel to the substrate.[37−40] Quite some effort has been taken to stabilize cylinders oriented perpendicular to the interfaces, which is often desired for further processing.[41−46]

In a previous Letter we presented a core−shell cylinder-forming triblock terpolymer [poly(styrene)-*block*-poly(2-vinylpyridine)-*block*-poly(*tert*-butyl methacrylate)] (PS-*b*-P2VP-*b*-PtBMA) showing a highly ordered perforated lamella structure in thin films.[47] This particular thin film structure is a potential candidate for future applications, it can, e.g., serve as a lithographic mask or a nanoporous membrane after selective removal of one of the components and can also be chemically converted into an amphiphilic structure without losing its order.

Here we compare the structure formation of the above-mentioned core−shell cylinder-forming PS-*b*-P2VP-*b*-PtBMA triblock terpolymer in solution and in thin films. In the latter case the samples are annealed in controlled solvent vapor atmosphere with the structure formation process taking place in concentrated solutions. We employ gradient combinatorial techniques which enable a systematic analysis of the film phase behavior in a single specimen. In addition to rapidly providing a comprehensive map of the phase behavior, such techniques reduce the problems of reproducibility since processing parameters are held constant. For instance, here we keep solution concentration and solvent exposure constant and vary film thickness and substrate interaction. Our aim is to understand and eventually control the rather complex phase behavior of triblock terpolymers.

Experimental Section

Molecular Characteristics. Using sequential living anionic polymerization we synthesized a series of monodisperse triblock terpolymers consisting of poly(styrene) (PS), poly(2-vinylpyridine) (P2VP), and poly(*tert*-butyl methacrylate) (PtBMA) with increasing molecular weight of the PtBMA block. Details about synthesis and bulk characterization have been described previously.[48] Table 1 summarizes the molecular parameters of the polymers investigated in the present contribution. Depending on the volume fraction of PtBMA the

* Corresponding authors. E-mail: (S.L.) sabine.ludwigs@uni-bayreuth.de and (G.K.) georg.krausch@uni-bayreuth.de.
† Physikalische Chemie II, Universität Bayreuth.
‡ National Institute of Standards and Technology (NIST).
§ Bayreuther Zentrum für Kolloide und Grenzflächen (BZKG), Universität Bayreuth.

10.1021/ma049048d CCC: $30.25 © 2005 American Chemical Society
Published on Web 02/03/2005

Table 1. Block Terpolymer Molecular Characteristics

polymer[a]	M_w [kg/mol]	M_w/M_n[b] (GPC)	$\phi_{PS}:\phi_{P2VP}:\phi_{PtBMA}$[b]	d_{SAXS} [nm][b]	morphology[c]
$S_{19}V_{25}T_{56}^{120}$	120	1.03	1:1.2:3.05	(71 ± 3) nm	G/PL/C
$S_{17}V_{22}T_{61}^{132}$	132	1.03	1:1.2:3.65	(74 ± 3) nm	G/PL/C
$S_{16}V_{21}T_{63}^{140}$	140	1.03	1:1.2:4	(72 ± 3) nm	C

[a] $S_{\%PS}V_{\%P2VP}T_{\%PtBMA}^{Mw}$ with the subscripts representing the weight fractions of the respective blocks (parts in hundred), while M_w is the total weight-averaged molecular weight in kg/mol. [b] Key: M_w/M_n, polydispersity determined with GPC; $\phi_{PS}:\phi_{P2VP}:\phi_{PtBMA}$, volume fraction; d_{SAXS}, bulk domain spacing determined with SAXS measurements. [c] Key: G, core−shell−gyroids; PL, perforated lamellae; C, core−shell cylinders.

materials in bulk form core−shell cylinders ($\phi_{PS}:\phi_{P2VP}:\phi_{PtBMA}$ = 1:1.2:4) and a coexistence of core−shell gyroids, core−shell cylinders, and what we assume to be a perforated lamella structure ($\phi_{PS}:\phi_{P2VP}:\phi_{PtBMA}$ = 1:1.2:3.05−3.65). In the following we denote the polymers as $S_xV_yT_z^{Mw}$ with the subscripts representing the weight fractions of the respective blocks (parts of hundred) and the superscript M_w indicating the total weight-averaged molecular weight in kg/mol. We will focus our investigations on the polymer with the highest amount of PtBMA, $S_{16}V_{21}T_{63}^{140}$, which forms in the bulk a well-defined core−shell cylinder structure with poly(styrene) forming the core surrounded by a shell of poly(2-vinylpyridine) within a matrix of poly(*tert*-butyl methacrylate).

Solutions of $S_{16}V_{21}T_{63}^{140}$ in both chloroform ($CHCl_3$) and tetrahydrofurane (THF) with different mass fractions w_P were investigated with small-angle X-ray scattering (SAXS). Synchrotron SAXS measurements were performed at the ID2 beamline at the European Synchrotron Radiation Facility (ESRF, Grenoble, France). All solutions were directly prepared in capillaries with about 2 mm diameter. The typical photon flux obtained at the ID2 sample position is 8×10^{12} photons/s; the energy bandwidth is $\Delta E/E = 2 \times 10^{-4}$. All experiments were obtained at 12.5 keV corresponding to an X-ray wavelength of 0.1 nm. The scattering intensities were detected via a CCD camera. The detector system is housed in a 10 m evacuated flight tube. The scattering patterns were corrected for the beam stop and the background prior to evaluations. The calculations of the scattering intensities were obtained with the Fit2D evaluation program.

Thin Film Sample Preparation. Thin films were cast onto polished silicon substrates from $CHCl_3$ solutions. The polymer solutions were placed between a glass blade located about 200 μm above a silicon substrate at a relative angle of 5°. The substrate was moved relative to the blade at constant acceleration, resulting in linear gradients in film thickness. Solutions with 1−2 wt % polymer resulted in a gradually increasing film thickness from 30 to 120 nm. The thickness variation was detected with an automated Filmetrics F20 UV−vis interferometer. For detailed information about preparation of gradients in film thickness, see ref 49. The as-prepared samples were subsequently annealed in a well-controlled atmosphere of $CHCl_3$ or THF vapor for several days to induce mobility and facilitate equilibration. Details of the experimental setup are described in ref 34. As the molecular weight of the investigated polymer is quite high (140 kg/mol), relatively high vapor pressures ($p_{CHCl3} = 0.9\ p_0$, $p_{THF} = 0.95\ p_0$, with p_0 being the vapor pressure of saturated $CHCl_3$ and THF, respectively) were needed to ensure a reproducible microstructure formation process in thin films.

After swelling in solvent vapor for a certain time interval the microdomains were frozen in via quenching with pure air. This results in a shrinking of the swollen film thickness. The samples were then investigated with light microscopy, field-emission scanning electron microscopy (FE-SEM) (LEO 1530), and scanning force microscopy (SFM) (Dimension 3100 Metrology SFM from Digital Instruments), which was operated in tapping mode. For SFM imaging we usually used light-tapping conditions with an amplitude set point A/A_0 being typically 0.98 and a free amplitude A_0 of about 20−30 nm. Scratches with a needle were made on the sample to enable imaging of the same spot with all techniques and facilitate step height measurements with SFM. While SFM is a nondestructive technique for surface investigations, it is well known that electron beam damage during SEM imaging can lead to considerable volume shrinkage of the polymethacrylate phase.[50] Using the in-lens detector of the SEM at a quite low accelerating voltage of 0.8 kV enables detection of a material contrast between the different components of the block copolymers.

Besides using pure silicon substrates, hydrophobic substrates were prepared by chemically grafting self-assembled monolayers (SAM) of trialkylsilanes onto silicon substrates. The SAM were prepared by reaction of monofunctional *n*-octyldimethylchlorosilane (ODS, >95% mass concentration, Gelest Inc, Tullytown, PA) with silicon wafers in the vapor phase. The surface energy of these different substrates can be evaluated by static contact angle measurements of water and diiodomethane. The water contact angle of pure SiO_x amounts to 40°, which results in a surface energy of ~60 mN/m, while the water contact angle of the SAM-modified substrate amounts to ~95°, resulting in ~26 mN/m.

Etching Methods. To establish the microdomain structure beneath the surface some films were investigated by Nanotomography.[51] For volume imaging ~7 nm thick layers of the block copolymer were successively removed by plasma etching, and tapping-mode SFM images were taken after each erosion step at the same spot of the sample. For plasma etching the thin film was placed in a Harrick PDC-32G Plasma Cleaner, which was then operated with pure oxygen plasma at 1.5 ± 0.1 mbar and 60W rf for 7s. The etching rates of the block components have been determined to v(PS) = 29.4 nm/min, v(P2VP) = 33.6 nm/min, v(PtBMA) = 63 nm/min. Alternatively, exposing the thin film to UV light (UV−B, 150 W, 60 min) and subsequent rinsing with *n*-hexane was used to selectively remove the methacrylate component.

Results and Discussion

Solution Behavior of $S_{16}V_{21}T_{63}^{140}$. Figure 1a and b show SAXS spectra of solutions of $S_{16}V_{21}T_{63}^{140}$ in $CHCl_3$ and THF, respectively, with polymer weight fractions w_P between 10 and 50 wt %. Above a certain concentration the SAXS spectra show Bragg peaks with relative positions of $1:\sqrt{3}:2:\sqrt{7}$ characteristic of hexagonally ordered cylinders. This finding is consistent with the hexagonal structure found for dry bulk samples cast from solution. From the SAXS spectra the order−disorder transition for THF solutions $w_{p,ODT,THF}$ can be located between 28.9 and 30 wt %. With additional birefringence experiments (not shown here) we determined the order−disorder transition for $CHCl_3$ solutions to $w_{p,ODT,CHCl3}$ = (26 ± 0.5) wt %. Figure 1c shows the domain spacing as a function of the polymer weight fraction. With increasing polymer weight fraction the domain spacing increases with a maximum value found for the melt spacing after solvent evaporation (w_p = 100%).

Structure Formation Process in Thin Films. Rather high vapor pressures of the solvent are needed for a reproducible structure formation in thin films. The degree of swelling during solvent vapor exposure can be determined with a spectroscopic ellipsometer.[53] At vapor pressures of $p_{CHCl3} = 0.9\ p_0$ the films swell to 2.5 times their dry thickness, resulting in polymer concentrations of w_p = 32.5 wt %. This concentration is above the determined order−disorder transition in bulk solu-

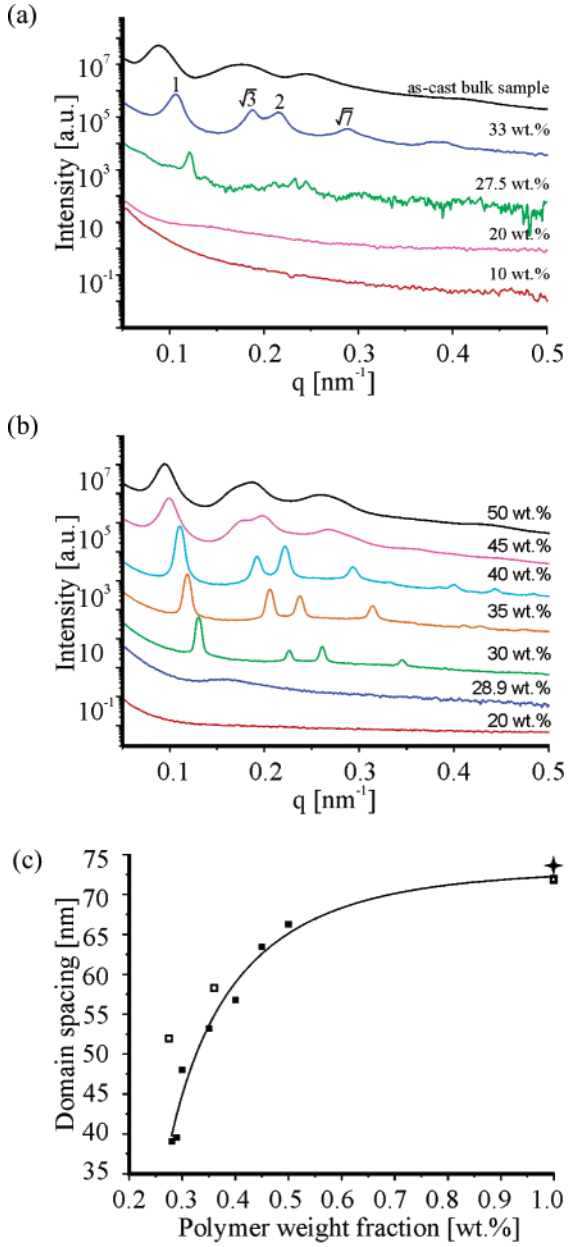

Figure 1. SAXS spectra of $S_{16}V_{21}T_{63}^{140}$ in $CHCl_3$ (a) and THF (b) solutions. (c) Domain spacing as function of the polymer weight fraction: open symbols correspond to $CHCl_3$ solutions, closed symbols represent THF solutions, the star marks the domain spacing of a $CHCl_3$–cast bulk sample. The line is a guide to the eye.

tions (Figure 1). In the swollen state the films are microphase separated and the structure formation process takes place in highly concentrated solutions. This has been verified with in-situ SFM experiments in the swollen state for a similar system.[34]

Accurate control of the vapor pressure and sufficiently long annealing times are indispensable for reproducible formation of ordered microdomain structures. As an example, Figure 2 a and b show ~40 nm thick films after insufficient annealing. In both cases the structures show little long-range order and appear to be unstable to further evolution in the presence of solvent vapor. The annealing times required to form equilibrium microdomain structures increase with increasing film thickness: For thin film gradients with thicknesses between 30 and 120 nm, annealing times of about 120 h are required to obtain stable structures.

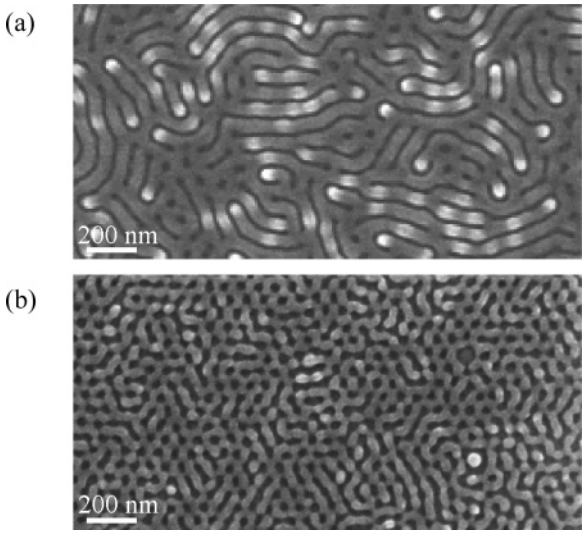

Figure 2. SEM micrographs of a ~40 nm thick film of $S_{16}V_{21}T_{63}^{140}$ after annealing in $CHCl_3$ vapor for (a) 10 and (b) 16 h.

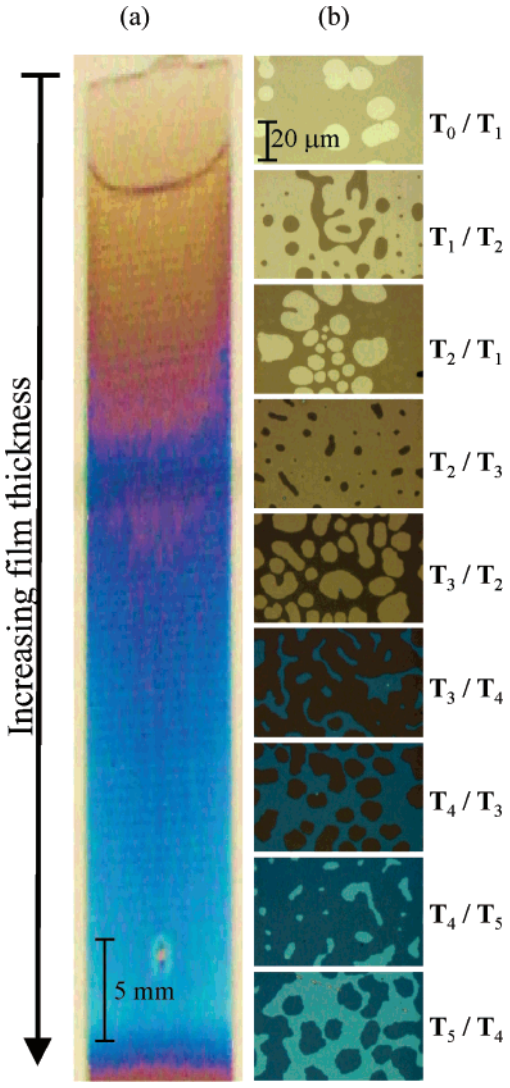

Figure 3. Optical micrographs of the film thickness gradient before (a) and after annealing in solvent vapor (b). The terraces are labeled from T_0 to T_5 with increasing film thickness.

Figure 3a shows an optical micrograph of a thin film of $S_{16}V_{21}T_{63}^{140}$ on a silicon substrate prior to annealing.

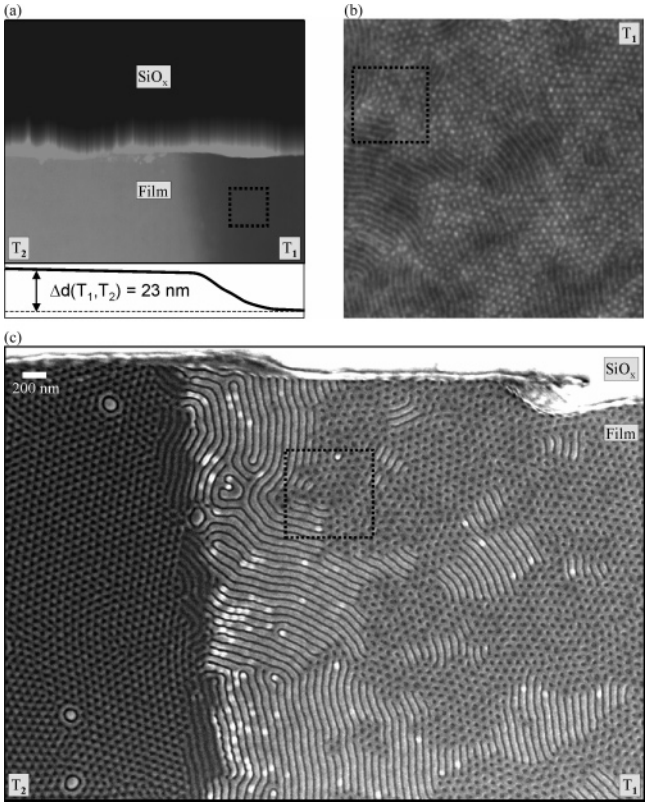

Figure 4. Images of a thin film of $S_{16}V_{21}T_{63}^{140}$ after exposure to $p_{CHCl3} = 0.9\ p_0$ for 120 h (with p_0 being the vapor pressure of saturated $CHCl_3$) taken with different techniques. (a) SFM topography image of a transition between T_1 and T_2 next to a scratch (image size, $6 \times 6\ \mu m^2$) together with the corresponding height profile, (b) higher magnification SFM topography image of T_1 (image size, $3 \times 3\ \mu m^2$), (c) SEM image of the same sample region; the black boxes indicate the same sample positions.

The film thickness increases from about 30 (at the top) to about 120 nm (at the bottom) over a lateral distance of about 10 cm. On annealing in $CHCl_3$ vapor ($p_{CHCl3} = 0.9\ p_0$, $t = 120$ h), the originally smooth gradient in film thickness develops terraces of uniform thickness characterized by uniform interference colors in the optical micrographs (Figure 3b). This finding suggests that the local thickness adjusts to local minima of the free energy of the system which are related to energetically preferred microdomain structures in the film.[53] The terrace formation is an unambiguous indication that the swollen films are microphase separated. In the following the terraces are denoted as T_0, T_1, T_2, T_3, T_4, and T_5 in the succession of increasing film thickness. The terraces show the same progression from holes to islands to smooth surface as a function of film thickness as found in other block copolymer systems.[23,53]

The terraced surface structures were investigated with scanning force microscopy and subsequent scanning electron microscopy at the same spot of the sample: Scratches with a needle were made to mark a particular sample region and enable height measurements with SFM. Figure 4a shows an example of a SFM height image of the slope between the neighboring terraces T_1 and T_2 next to a scratch down to the pure silicon substrate together with a cross-section corresponding to the height difference between T_1 and T_2. The local film thickness d was determined with the step height feature of the Nanoscope III software and amounts to $d_{T1} \approx 35$ nm for the first terrace, $d_{T2} \approx 58$ nm for the second terrace, and $\Delta d(T_1,T_2) \approx 23$ nm for the thickness difference between the two terraces. Figure 4b shows the height image of T_1 with a higher magnification. The topography is still very smooth; the difference between peaks and valleys amounts to ~2 nm. Figure 4c finally exhibits the corresponding SEM image of the same region (compare the identically located boxes in Figure 4a, b, and c which show clearly resolved stripe-like and dot-like patterns. The left part of the SEM image (T_2) appears darker than the right part (T_1). At the SEM operating conditions chosen here (acceleration voltage ≈ 0.8 kV) we find quite consistently that the secondary electron yield from thicker regions of the films is smaller than that from thinner regions, resulting in the observed "color" differences in the SEM images. At these low electron energies the thickness of the insulating polymer layer seems to have a profound effect on the secondary electron yield. This effect is smaller at steps between higher terraces (thicker films).

Thin Film Phase Behavior of $S_{16}V_{21}T_{63}^{140}$, Annealed in $CHCl_3$ Vapor. In this section we systematically investigate the morphology as a function of the film thickness for a thin film of $S_{16}V_{21}T_{63}^{140}$ prepared on a hydrophilic substrate (SiO_x) after annealing in $CHCl_3$ vapor ($p_{CHCl3} = 0.9\ p_0$, $t = 120$ h). In a second experiment we perform the same experiment on a hydrophobic substrate to test the stability of the structure to variations of substrate conditions, surface energy being an important substrate parameter.

In Figure 5a we summarize the development of the film thickness with increasing step height from terrace T_0 to T_5 for a thin film prepared on SiO_x. The thickness values are determined from SFM height images of neighboring terraces and subsequently merged. The film thickness as a function of the terrace number is displayed in Figure 5b. The open circles in Figure 5b correspond to terraces observed on SiO_x. The heights increase linearly with the number of layers in the film. The first terrace exhibits a film thickness of $d_{T0} \approx 11 \pm 2$ nm. The offset corroborates the existence of a wetting layer with a thickness of $d_{T0} \approx 11 \pm 2$ nm underneath the terraces T_1 to T_5. The height differences between the remaining terraces were found to have a constant value of $\Delta d \approx 23 \pm 2$ nm. For both islands and holes the individual terraces have the same thickness within the experimental error of 2 nm.

The scanning electron micrographs (Figure 5c) exhibit the following sequence of structures: The regions with the lowest film thickness (T_0) show a disordered structure (dis), followed by a liquidlike distribution of dots (bright dots) which may be assigned to perpendicularly oriented PS/P2VP-cylinders in a PtBMA matrix ($C_\perp$). The stripe-like pattern can be identified as cylinders aligned parallel to the plane of the film ($C_{||}$). The terraces show a hexagonal arrangement of dark dots, which are identified as a perforated lamella (PL). For a detailed discussion of the PL phase, see below. The slopes between adjacent terraces exhibit $C_{||}$ between T_1 and T_2 and a coexistence of $C_{||}$ and PL between T_2 and T_3 and between T_3 and T_4. At larger film thickness, the perforated lamella phase is observed throughout the entire thickness range as surface structure (see, e.g., between T_4 and T_5).

Scanning force microscopy height images of the PL phase exhibit a rather smooth surface topography which can be explained by a thin layer of the matrix phase

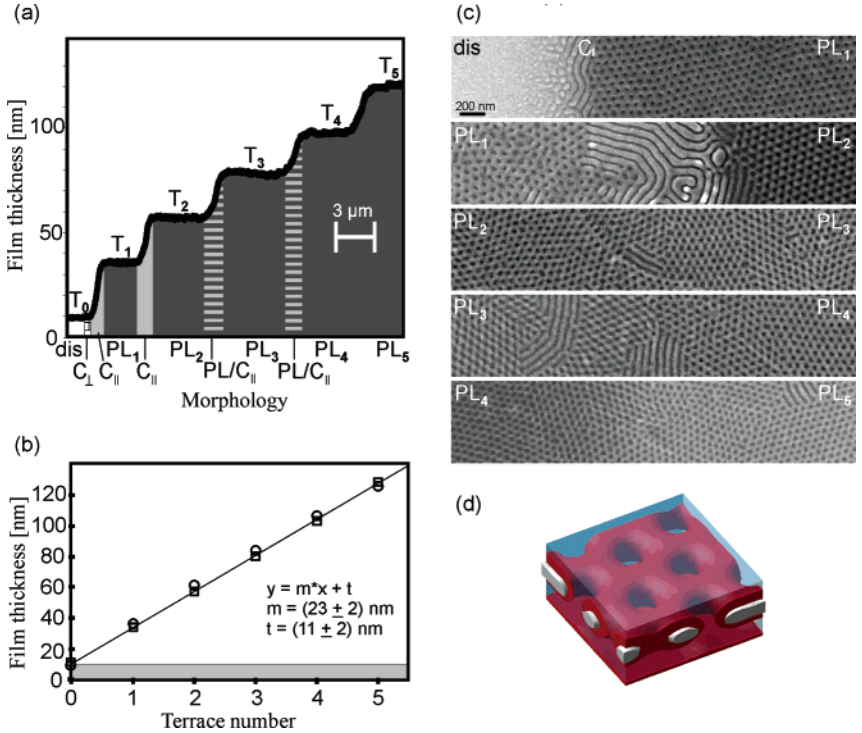

Figure 5. Thin film phase behavior of a thin film of $S_{16}V_{21}T_{63}^{140}$ ($p_{CHCl3} = 0.9\ p_o$, $t = 120$ h). (a) Height profiles between neighboring terraces (measured with SFM) which are merged laterally. The transitions from T_0 to T_1, from T_1 to T_2, from T_2 to T_3, from T_3 to T_4, and from T_4 to T_5 are shown. (b) Film thickness as function of the terrace number: the circles represent terraces formed on hydrophilic substrates (SiO_x), the boxes represent terraces formed on hydrophobic substrates (SAM); the height of the symbols includes the error bar. (c) Corresponding SEM images of the same sample regions. The terrace structures can be assigned to perforated lamellae (PL). (d) MesoDyn simulation of the first terrace of perforated lamellae; the phases can be assigned to PS (white phase), P2VP (red phase), and PtBMA (blue phase).[47]

poly(*tert*-butyl methacrylate) at the air/film interface. PtBMA is the component with the lowest surface energy and preferentially accumulates at the air surface: γ_{PS} = 41 mN/m,[54] γ_{P2VP} = 40 mN/m,[55] γ_{PtBMA} = 30.5 mN/m.[54] We attribute the corrugations which typically amount 2 nm to small differences in the degree of shrinking during the sample preparation process. The scanning electron micrographs reveal a clearly resolved hexagonal arrangement of dark dots, because the topmost layer of the methacrylic ester is removed upon exposure to the electron beam. Similarly, upon exposure of the film to UV light the top 7 nm of the thin film are removed and a hexagonal array of holes develops beneath the originally rather flat surface, which can also be imaged with SFM. Figure 6 shows SFM images prior to (a) and after exposure to UV irradiation (b). Etching in an oxygen plasma can be used for volume imaging of one layer of PL: After three etching steps (Figure 6 (c) after 15 s, (d) after 75 s, (e) after 135 s) and removal of an approximately ~30 nm thick layer ($d_{T1} \approx 35 \pm 2$) nm a hexagonal array of holes is still visible in the scanning force microscopy height image. This finding is attributed to the higher etching rate of PtBMA compared to the other two blocks. The (*tert*-butyl methacrylate) group is a very labile group. Upon etching in the oxygen plasma these labile linkages are broken and small species are vaporized in the plasma.[56] Further etching did not change the structure and the film thickness. The wetting layer beneath the PL phase cannot be resolved in this manner. This may be explained by a chemical cross-linking process of the polymers, as especially poly(styrene) and poly(2-vinylpyridine) tend to cross-link in the presence of radicals. This makes it also impossible to investigate thicker terraces of PL.

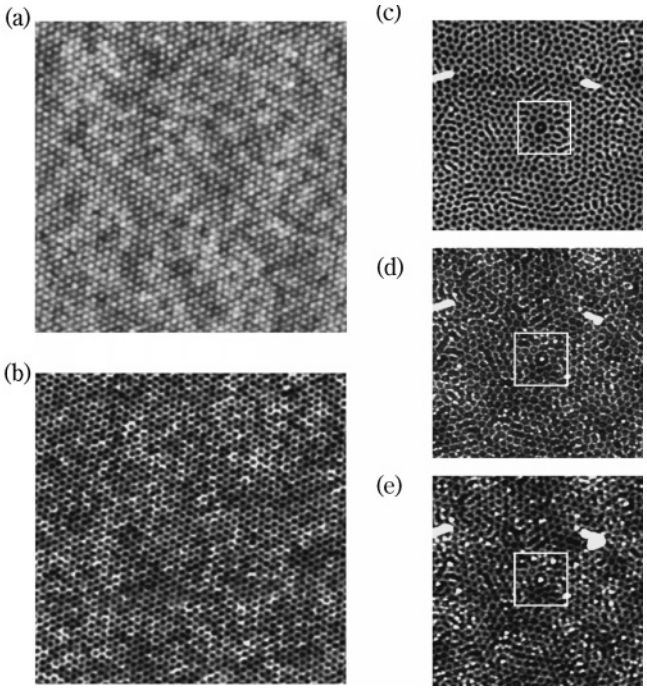

Figure 6. SFM images of a perforated lamella structure. Before (a) and after (b) exposure to UV light for 10 min. Image size, 3 × 3 μm^2; height scale, Δz = 0−10 nm. (c−e) Layer-by-layer imaging: SFM images after 15 (c), 75 (d), and 135 s (e) etching in oxygen plasma. Image size, 2 × 2 μm^2; height scale, Δz = 0−10 nm.

The PL phase can be visualized as a P2VP/PS/P2VP sheet perforated by PtBMA channels, which connect between two outer PtBMA layers. The experimental

results are supported by recent calculations based on the dynamic density functional theory (DDFT) using the MesoDyn code.[47] Figure 5d shows a sketch of the first terrace of PL. The PtBMA majority phase has the lowest surface energy and therefore is attracted to the free surface of the film. We assume that due to the particular stoichiometry of the block copolymer ($\phi_{PtBMA} = 61$ vol %) the wetting layer next to the substrate is terminated by a PtBMA-rich surface, which can also attract PtBMA. As a consequence the perforated lamella phase is stabilized between two interfaces both attracting the majority component of the polymer. In the experiments, in the case of the polar SiO_x substrate, the wetting layer ($d_{T0} \approx 11$ nm) is attributed to a thin, laterally homogeneous layer of polymer chains physisorbed from solution via the most polar block poly(2-vinylpyridine) block.[57] Fukunaga et al. have shown that poly(styrene)-*b*-poly(2-vinylpyridine)-*b*-poly(*tert*-butyl methacrylate) is pinned with P2VP onto SiO_x substrates with PtBMA forming a uniform layer on top.[58,59]

Effect of Substrate Surface Energy. Figure 5b includes the thickness values obtained for thin films prepared at the hydrophobic extreme value, i.e., untreated self-assembled monolayers (SAM; water contact angle, 95°). The heights increase linearly with the number of layers in the film. As the values identically track values observed on the hydrophilic SiO_x substrate, we conclude that the substrate surface energy does not affect the film thickness of the individual terraces. The offset d_{T0} corroborates the existence of a wetting layer. On a hydrophobic substrate we assume that PS is attracted by the substrate and PtBMA forms a layer on top, as poly(styrene) is the least polar block. As the surface structures and the film heights are the same on hydrophilic and hydrophobic substrates, we assume a half-lamella layer terminating with poly(*tert*-butyl methacrylate). Removing the thin film from the substrate and investigating the bottom of the film could probably help to resolve the structure of the thinnest layer. The majority component PtBMA ($\phi_{PtBMA} = 61$ vol %) forms the uniform top layer of this wetting layer, both on hydrophilic and hydrophobic substrates. For different surface energies PS, P2VP, or both are present at the substrate. We assume that the influence of the substrate is screened by this wetting layer. This is supported by computer simulations of Lyakhova et al.[36] and Ludwigs et al.[60]

In summary, we found four characteristic patterns at the film surface irrespective of the substrate nature: A rather featureless pattern, which we identify as disordered phase (dis), upright standing cylinders ($C_\perp$), cylinders oriented parallel to the surfaces ($C_{||}$), and perforated lamellae (PL) at the terraces. Considering the terrace heights and the thickness of the wetting layer beneath all terraces ($d_{T0} \approx 11$ nm), we anticipate that layers of PL with a natural domain size of $\Delta d \approx 23 \pm 2$ nm are stacked on top of each other; however, there is no direct experimental evidence for this. The slopes between the first terraces are formed of $C_{||}$; with increasing film thickness we also find PL between the terraces. This phenomenon is explained with confinement effects which play a nonnegligible role in one or two microdomain thick layers, while they are much smaller in thicker films.

Similar surface structures have been recently found in cylinder-forming SBS block copolymers.[23,34−36] With increasing film thickness both experiments and simulations showed a disordered phase for the smallest thickness, very short upright cylinders $C_\perp$, parallel cylinders $C_{||}$, and perforated lamellae PL. The phase transitions occurred at well-defined film thicknesses with $C_{||}$ being formed on the terraces. Our results can be compared to this behavior only to some extent. While the phase behavior of SBS is dominated by the bulk structure ($C_{||}$ and $C_\perp$), we find the PL as dominating surface structure of a core−shell cylinder-forming system. In analogy to the SBS system, we can assign the dot-like structure (bright dots) to very short cylinders oriented perpendicular to the surfaces ($C_\perp$), though a clear hexagonal arrangement is not observed in the SEM images.

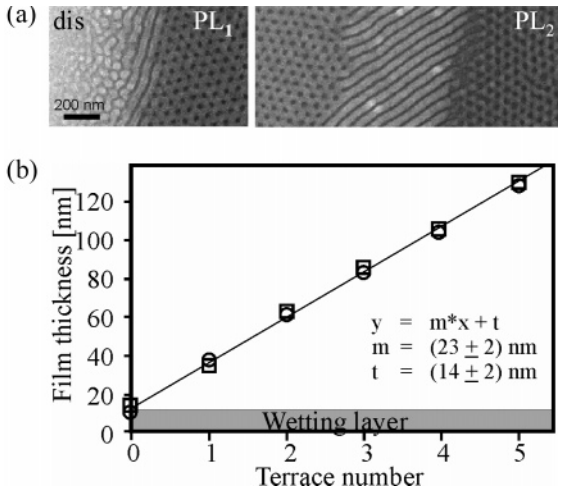

Figure 7. Thin films of $S_{17}V_{22}T_{61}^{132}$ and $S_{19}V_{25}T_{56}^{120}$ after exposure to $CHCl_3$ vapor ($p_{CHCl3} = 0.9p_0$, $t = 100$ h). (a) SEM images of the transition between T_0-T_1 and T_1-T_2 of a thin film of $S_{17}V_{22}T_{61}^{132}$. (b) Film thickness as function of the terrace number: circles represent thickness values observed for $S_{17}V_{22}T_{61}^{132}$, and squares represent values observed for $S_{19}V_{25}T_{56}^{120}$. The height of the symbols includes the error bar.

Comparison with Thin Film Phase Behavior of $S_{17}V_{22}T_{61}^{132}$ and $S_{19}V_{25}T_{56}^{120}$. In the previous section we focused on the thin film phase behavior of $S_{16}V_{21}T_{63}^{140}$ which shows a core−shell cylinder structure in bulk. Decreasing the volume fraction of PtBMA toward a symmetric composition we identify a composition region in the phase diagram which exhibits a coexistence of core−shell gyroids, core−shell cylinders, and perforated lamellae. The polymers and their molecular parameters are listed in Table 1. The investigation of thin films of these polymers prepared in the manner described above exhibits the same sequence of surface structures with gradually increasing film thickness as the core−shell cylinder phase. Again, the PL phase dominates the phase behavior in thin films. Figure 7a shows the terrace transitions from T_0 to T_2 for $S_{17}V_{22}T_{61}^{132}$ after exposure to $p_{CHCl3} = 0.9\ p_o$ for 120 h. The film thickness dependent on the terrace number is shown in Figure 7b. The terraces measured for $S_{19}V_{25}T_{56}^{120}$ (circles) and $S_{17}V_{22}T_{61}^{132}$ exhibit similar thickness values which amount to $\Delta d(T_1,T_2) \approx (23 \pm 2)$ nm; the wetting layer amounts to $d_{T0} \approx (14 \pm 2)$ nm. The thickness values do not differ significantly from the data observed for the core−shell cylinder system, $S_{16}V_{21}T_{63}^{140}$. This is not surprising as the SAXS data also show similar values for the bulk domain spacing, see Table 1.

Comparison with Thin Film Phase Behavior of $S_{16}V_{21}T_{63}^{140}$, Annealed in THF Vapor. We further investigated thin film specimens of $S_{16}V_{21}T_{63}^{140}$ on silicon wafers after annealing in THF vapor ($p_{THF} = 0.95$

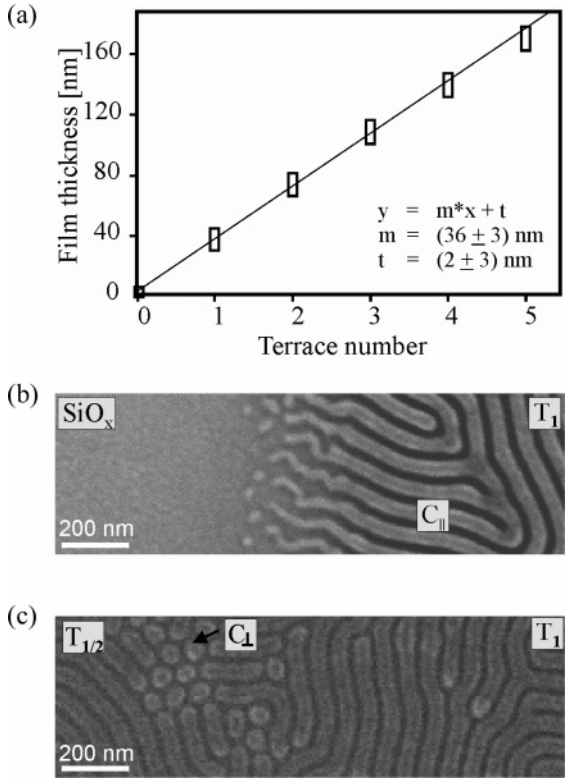

Figure 8. Thin film of $S_{16}V_{21}T_{63}^{140}$ after exposure to THF vapor ($p_{THF} = 0.95p_0$, 120 h. (a) Film thickness as function of the terrace number. The height of the symbols includes the error bar. (b and c) SEM micrographs of the transition from the silicon substrate to T_1 (b) and the transition between $T_{1/2}$ and T_1 (c).

p_o, 120 h). Figure 8a shows the film thickness as function of the terrace number. The thickness of the higher terraces amounts to integer multiples of the first terrace—T_1—with a value of $d_{T1} \approx 36 \pm 3$ nm. The terraces exhibit stripe patterns which are assigned to cylinders oriented parallel to the substrate. From scanning electron micrographs we assume a core−shell morphology with a PS core (dark gray) and P2VP shell (light gray) in a matrix of PtBMA (dark). In the thinnest regions of the sample we find two different sample areas: in some parts of the sample the first terrace T_1 is formed next to areas where no polymer film is left (pure SiO_x) (Figure 8b), and in other parts terraces with a thickness of $d_{T/2} \approx 20$ nm can be detected (Figure 8c). The latter corresponds to $T_{1/2}$ and exhibits cylinders oriented parallel to the substrate ($C_{||}$) as well as a small amount of hexagonally ordered bright dots which can be assigned to perpendicularly oriented cylinders ($C_\perp$).

In contrast to samples prepared in $CHCl_3$ vapor, no transition from a core−shell cylinder structure in bulk to perforated lamellae in thin films is found after preparation in THF vapor. All terraces and transitions show cylinders. The surface field apparently causes the cylinders to orient parallel to the substrate. The cylinders seem to adjust themselves to a thickness corresponding to the instantaneous thickness during the swelling process.

Recently Elbs et al. used spectroscopic ellipsometry to determine the swelling behavior of thin films of the homopolymers PS, P2VP, and PtBMA in controlled atmosphere of $CHCl_3$ and THF.[52] From the degree of swelling as a function of the solvent vapor pressure they could estimate Flory−Huggins interaction parameters between polymers and solvents. They found that the rather polar solvent $CHCl_3$ swells P2VP more and the nonpolar polymer PS less. THF turned out to be almost nonselective; hardly any difference in the degree of swelling between the three homopolymers could be detected. Therefore, they expected the thin film phase diagrams of the triblock terpolymers to be slightly different in the different solvents. Briefly, their thin film investigations show the following results:[61] samples annealed in THF vapor exhibited the tendency of forming cylinders oriented parallel to the surface—which is in accordance with our present results. Exposure to $CHCl_3$ vapor led to structures with a smaller mean curvature, which they assumed to be gyroid-like and show perforated lamellae with our experimental route. Their sample preparation was based on swelling thin films of $S_{17}V_{26}T_{57}^{110}$ in solvent vapor and slowly extracting the solvent by decreasing the solvent vapor pressure. During solvent evaporation the concentration of the polymer solutions increases, and at high concentrations the relaxation time of the polymer solution can eventually reach the time scale of the preparation process and the respective morphology will be frozen. In the present contribution we used an improved method of sample preparation. We anneal our samples well above the order−disorder transition in the ordered (microphase separated) state in a controlled atmosphere of solvent vapor at a defined vapor pressure, which results in swelling of the films to about 2.5 times of their original dry thickness. The structure formation process takes place in these high concentrated solutions. Via quenching the films by evaporation of the high vapor pressure solvent in pure air, the films shrink in the z-direction and the respective microdomain structures are frozen in. In contrast to Elbs et al., we work with controlled solvent vapor pressures and fast extraction rates which were shown not to influence the microdomain structures.[34] Despite the influence of preparation, Elbs et al. observed similar tendencies of structure formation in $CHCl_3$ and THF. Regarding the bulk and solution data, the difference in selectivity obviously does not affect microdomain formation: a cylindrical phase is formed in both solvents. In thin films the additional interfaces and confinement of the material to the bulk domain spacing stabilize surface reconstructions, mostly perforated lamellae after annealing in a slightly selective solvent, like $CHCl_3$. The thin film phase behavior of films annealed in THF is dominated by the bulk structure.

Additional Complex Thin Film Structures. In addition to our systematic findings about the relationship between the morphology and the film thickness, we finally give an idea of the complexity of the phase behavior of ABC triblock terpolymers in thin films. We already underlined the importance of a well-defined sample preparation in the previous sections. Figure 9 shows surface structures found on one single film of $S_{17}V_{22}T_{61}^{132}$ after exposing it to $CHCl_3$ vapor for 50 h. The sample was prepared in an experimental setup where the vapor pressure could slightly vary because of changes in the temperature of the environment ($p_{CHCl3} \approx 0{,}9p_0$). We were unable to reproduce this particular sample preparation. In Figure 9a a SEM image of the first terrace of a modified perforated lamella phase next to cylinders oriented parallel to the surfaces is displayed. As the PL phase pattern differs from that of Figures 4 and 5, we performed scanning

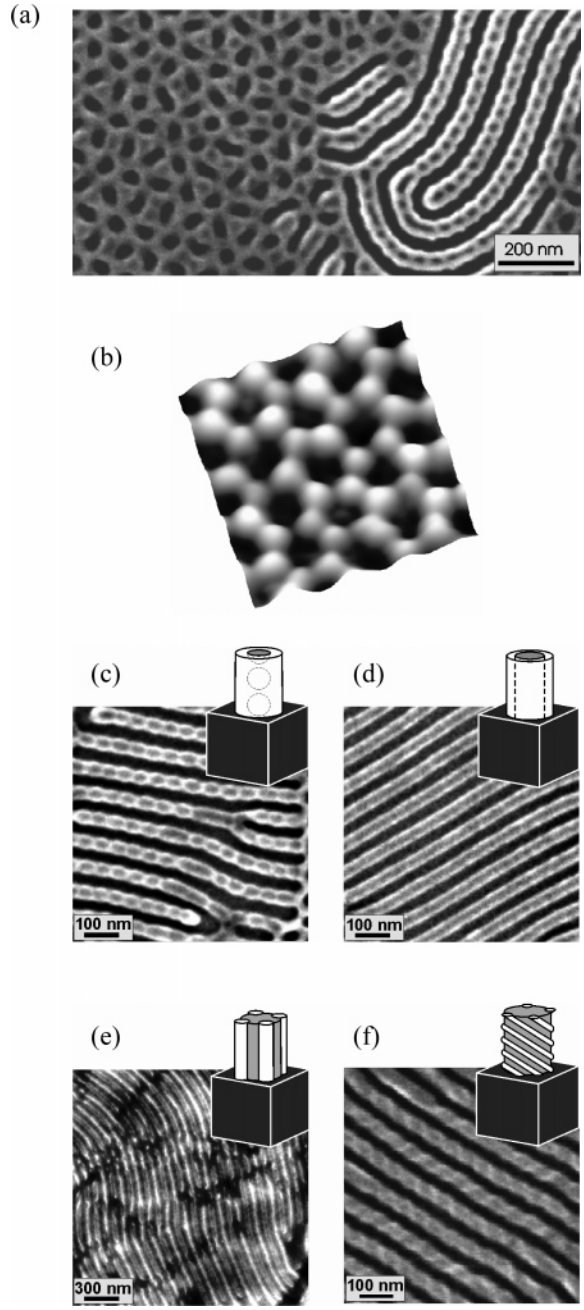

Figure 9. Surface structures found on one thin film of $S_{17}V_{22}T_{61}^{132}$ after preparation in $CHCl_3$ vapor ($p_{CHCl3} \approx 0.9p_0$, 50 h). (a) SEM image of the transition between perforated lamellae (T_1) and a sphere-in-cylinder morphology. (b) SFM image of T_1 after removing a layer of ~7 nm in oxygen plasma (300×300 nm^2, the height difference between the protrusions and holes amounts to around 4 nm). (c–f) SEM images of different cylinder morphologies: sphere-in-cylinder morphology (c), core–shell–cylinders (d), cylinders-at-cylinders (e) and helix-around cylinder morphology (f). The sketches are adapted from ref 61. Color code: light gray corresponds to PS, gray to P2VP, dark gray to PtBMA.

force microscopy on a similar sample position. Figure 9b shows a SFM image after removing a layer of ~7 nm thickness in oxygen plasma. Around dark holes which are assigned to PtBMA perforations six gray protrusions are formed. The skeleton of the perforated lamella phase seems to be modified. We assume that the PS block does not form a continuous core but rather breaks into isolated PS microdomains embedded within P2VP. This is analogous to the cylinders found in the right part of Figure 9a and c. They can be assigned to a sphere-in-cylinder structure with isolated PS microdomains (dark gray in the image) embedded within P2VP cylinders surrounded by a continuous matrix of the majority component PtBMA. Other cylindrical structures found on the same sample are displayed in Figure 9d, e, and f: a familiar core–shell cylindrical structure (PS-core, P2VP-shell, PtBMA matrix), (d); a cylinder-(P2VP)-at-cylinder (PS) morphology; and a helix (P2VP)-around-cylinder (PS) morphology.

The sketches have been taken from Elbs et al., who have first seen these structures in thin films of $S_{17}V_{26}T_{57}^{110}$ prepared in THF vapor.[61] The corresponding bulk structures were first published by Stadler and co-workers.[25,62]

We assume that the coexistence of these different cylinder morphologies results from fluctuations in the polymer concentration during the annealing process in solvent vapor. We already mentioned that solvent annealing is a crucial point for structure formation. Even the smallest differences may induce transitions between neighboring structures. The core–shell structure arises, for example, from the sphere-in-cylinder morphology by merging the isolated PS spheres into a continuous PS cylinder. While the overall cylinder structure does not change, the microphase separation between the first blocks is apparently very sensitive to concentration fluctuations.

We emphasize through these examples the rich variety of surface structures possible in thin films of ABC triblock terpolymers. We expect these structures can reproducibly be formed under well-controlled conditions, either under equilibrium conditions (steady state, e.g., constant solvent vapor) or perhaps only under controlled processing conditions (e.g., solvent vapor ramps or controlled evaporation rates). Combinatorial methods are aptly suited for either route of future studies.

Conclusion

We apply a gradient combinatorial approach to the investigation of thin film structures of ABC triblock terpolymers consisting of poly(styrene), poly(2-vinylpyridine), and poly(*tert*-butyl methacrylate) in the stoichiometric range of $\phi_{PS}:\phi_{P2VP}:\phi_{PtBMA} = 1:1.2:3.05-4$. With gradients in films thickness we find a systematic dependence between the morphology and the film thickness. Terraces of well-defined film thickness exhibiting a perforated lamella structure are formed after annealing in a well-controlled atmosphere of nearly saturated $CHCl_3$ vapor. Due to the chemical nature of the block components and the particular stoichiometry of the polymer, a wetting layer with a PtBMA-rich top layer is formed next to the substrate. Irrespective of the nature of the substrate, the perforated lamella phase develops as the influence of the substrate is screened by the wetting layer.

The nature of the solvent used for annealing is shown to have a significant influence on the structure formation. While the same structure is observed in bulk and solution, confinement of the material to a certain film thickness induces a morphological phase transition: Using the same preparation procedure as with $CHCl_3$, use of THF leads to terraces exhibiting cylinders oriented parallel to the surfaces. No perforated lamella phase is formed at any film thickness. This phenomenon may be explained by a slight selectivity of $CHCl_3$ for P2VP, while THF appears to be nonselective for all blocks.

We finally emphasize the importance of a well-controlled atmosphere of solvent vapor for the annealing process. As the structure formation process takes place in highly concentrated polymer solutions, even slight changes in concentration may induce phase transitions between neighboring morphologies. Thin films of triblock terpolymers can exhibit a wealth of structures due to the delicate interplay between the large number of block−block and block−surface interactions. This complex phase behavior in thin films can be corroborated by computer simulations, which are presented in the accompanying paper.[60]

Acknowledgment. We thank C. Abetz for SEM measurements, M. Hund for help with etching experiments, C. Thunig for help with ODT measurements, and A. Knoll for fruitful discussions. We acknowledge support from the Deutsche Forschungsgemeinschaft (SFB 481), and R.M. acknowledges support from the VolkswagenStiftung.

References and Notes

(1) Bates, F. S.; Fredrickson, G. H. *Annu. Rev. Phys. Chem.* **1990**, *41*, 525.
(2) Bates, F. S.; Fredrickson, G. H. *Phys. Today* **1999**, *52*, 32.
(3) Hamley, I. W. *The Physics of Block Copolymers*; Oxford University Press: Oxford, 1998.
(4) Mansky, P.; Chaikin, P.; Thomas, E. L. *J. Mater. Sci.* **1995**, *30*, 1987.
(5) Mansky, P.; Harrison, C. K.; Chaikin, P. M.; Register, R. A.; Yao, N. *Appl. Phys. Lett.* **1996**, *68*, 2586.
(6) Park, M.; Harrison, C.; Chaikin, P. M.; Register, R. A.; Adamson, D. H. *Science* **1997**, *276*, 1401.
(7) Park, C.; Yoon, J.; Thomas, E. L. *Polymer* **2003**, *44*, 6725.
(8) Riess, G.; Hurtrez, G.; Bahadur, P. *Encyclopedia of Polymer Science and Engineering*; Wiley: New York, 1985.
(9) Auschra, C.; Stadler, R. *Polym. Bull.* **1993**, *26*, 2171.
(10) Yagci, Y.; Mishra, M. K. *The Polymeric Materials Encyclopedia*; CRC Press: Boca Raton, FL, 1996.
(11) Matyjaszewski, K. *Curr. Opin. Solid State Mater. Sci*. **1996**, *1*, 769.
(12) Leibler, L. *Macromolecules* **1980**, *13*, 1602.
(13) Helfand, E.; Wasserman, Z. R. *Macromolecules* **1980**, *13*, 994.
(14) Semenov, A. N. *Sov. Phys.* **1985**, *JETP 61*, 733.
(15) Meier, D. J. *Thermoplastic Elastomers*; Carl Hanser Verlag: München, 1987.
(16) Nakazawa, H.; Ohta, T. *Macromolecules* **1993**, *26*, 5503.
(17) Matsen, M. W.; Bates, F. S. *Macromolecules* **1996**, *29*, 1091.
(18) Matsen, M. W.; Bates, F. S. *J. Chem. Phys.* **1997**, *106*, 2436.
(19) Fredrickson, G. H.; Ganesan, V.; Drolet, F. *Macromolecules* **2002**, *35*, 16.
(20) Drolet, F.; Fredrickson, G. H. *Phys. Rev. Lett.* **1999**, *83*, 4317.
(21) Pickett, G. T.; Balazs, A. C. *Macromol. Theory Simul.* **1998**, *7*, 249.
(22) Huinink, H. P.; van Dijk, M. A.; Brokken-Zijp, J. C. M.; Sevink, G. J. A. *Macromolecules* **2001**, *34*, 5325.
(23) Knoll, A.; Horvat, A.; Lyakhova, K. S.; Krausch, G.; Sevink, G. J. A.; Zvelindovsky, A. V.; Magerle, R. *Phys. Rev. Lett.* **2002**, *89*, 035501.
(24) Zhang, W.; Wang, Z. G. *Macromolecules* **1995**, *28*, 7215.
(25) Stadler, R.; Auschra, C.; Beckmann, J.; Krappe, U.; Voigt-Martin, I.; Leibler, L. *Macromolecules* **1995**, *28*, 3080.
(26) Krausch, G. *Mater. Sci. Eng. Rep.* **1995**, *14*, 1.
(27) Fasolka, M. J.; Mayes, A. M. *Annu. Rev. Mater. Res.* **2001**, *31*, 323.
(28) Krausch, G.; Magerle, R. *Adv. Mater.* **2002**, *21*, 1579.
(29) Karim, A.; Singh, N.; Sikka, M.; Bates, F. S.; Dozier, W. D.; Felcher, G. P. *J. Chem. Phys.* **1994**, *100*, 1620.
(30) Radzilowski, L. H.; Carvalho, B. L.; Thomas, E. L. *J. Polym. Sci., Part B: Polym. Phys.* **1996**, *34*, 3081.
(31) Harrison, C.; Park, M.; Chaikin, P. M.; Register, R. A.; Adamson, D. H.; Yao, N. *Macromolecules* **1998**, *31*, 2185.
(32) Zhang, Q.; Tsui, O. K. C.; Du, B.; Zhang, F.; Tang, T.; He, T. *Macromolecules* **2000**, *33*, 9561.
(33) Konrad, M.; Knoll, A.; Krausch, G.; Magerle, R. *Macromolecules* **2000**, *33*, 5518.
(34) Knoll, A.; Magerle, R.; Krausch, G. *J. Chem. Phys.* **2004**, *120*, 1105.
(35) Horvat, A.; Lyakhova, K. S.; Sevink, G. J. A.; Zvelindovsky, A. V.; Magerle, R. *J. Chem. Phys.* **2004**, *120*, 1117.
(36) Lyakhova, K. S.; Sevink, G. J. A.; Zvelindovsky, A. V.; Horvat, A.; Magerle, R. *J. Chem. Phys.* **2004**, *120*, 1127.
(37) van Dijk, M. A.; van den Berg, R. *Macromolecules* **1995**, *28*, 6773.
(38) Magonov, S. N.; Cleveland, J.; Elings, V.; Denley, D.; Whangbo, M.-H. *Surf. Sci.* **1997**, *389*, 201.
(39) Kim, G.; Libera, M. *Macromolecules* **1998**, *31*, 2670.
(40) Kim, G.; Libera, M. *Macromolecules* **1998**, *31*, 2569.
(41) Mansky, P.; Liu, Y.; Huang, E.; Russell, T. P.; Hawker, C. J. *Science* **1997**, *275*, 1458.
(42) Thurn-Albrecht, T.; Schotter, J.; Kastle, G. A.; Emley, N.; Shibauchi, T.; Krusin-Elbaum, L.; Guarini, K.; Black, C. T.; Tuominen, M. T.; Russell, T. P. *Science* **2000**, *290*, 2126.
(43) Jeoung, E.; Galow, T. H.; Schotter, J.; Bal, M.; Ursache, A.; Tuominen, M. T.; Stafford, C. M.; Russell, T. P.; Rotello, V. M. *Langmuir* **2001**, *17*, 6369.
(44) Guarini, K. W.; Black, C. T.; Yeung, S. H. I. *Adv. Mater.* **2002**, *14*, 1290.
(45) Jeoung, U.; Ryu, D. Y.; Kim, J. K.; Kim, D. H.; Russell, T. P.; Hawker, C. J. *Adv. Mater.* **2003**, *15*, 1247.
(46) Kim, S. H.; Misner, M. J.; Xu, T.; Kimura, M.; Russell, T. P. *Adv. Mater.* **2004**, *16*, 226.
(47) Ludwigs, S.; Böker, A.; Voronov, A.; Rehse, N.; Magerle, R.; Krausch, G. *Nat. Mater.* **2003**, *2*, 744.
(48) Ludwigs, S.; Böker, A.; Abetz, V.; Müller, A. H. E.; Krausch, G. *Polymer* **2003**, *44*, 6815.
(49) Meredith, J. C.; Smith, A. P.; Karim, A.; Amis, E. J. *Macromolecules* **2000**, *33*, 9747.
(50) Sawyer, L. C.; Grubb, D. T. *Polymer Microscopy*, 2nd ed.; Chapman & Hall: London, 1996.
(51) Magerle, R. *Phys. Rev. Lett.* **2000**, *85*, 2749.
(52) Elbs, H. Ph.D. Thesis, Bayreuth, 2001.
(53) Coulon, G.; Russell, T. P.; Deline, V. R.; Green, P. F. *Macromolecules* **1989**, *22*, 2581.
(54) Mark, J. E. *Physical Properties of Polymers Handbook*; American Institute of Physics: Woodbury, 1996.
(55) Ishizu, K.; Yamada, Y.; Fukutomi, T. *Polymer* **1990**, *31*, 2047.
(56) Grassie, N.; Scott, G. *Polymer Degradation and Stabilisation*; Cambridge University Press: Cambridge, 1988.
(57) Tassin, J. F.; Siemens, R. L.; Tang, W. T.; Hadziioannou, G.; Smith, B. A. *J. Phys. Chem.* **1989**, *93*, 2106.
(58) Fukunaga, K.; Elbs, H.; Magerle, R.; Krausch, G. *Macromolecules* **2000**, *33*, 947.
(59) Fukunaga, K.; Hashimoto, T.; Elbs, H.; Krausch, G. *Macromolecules* **2003**, *36*, 2852.
(60) Ludwigs, S.; Zvelindovsky, A. V.; Sevink, G. J. A.; Krausch, G.; Magerle, R. *Macromolecules* **2005**, *38*, 1859.
(61) Elbs, H.; Drummer, C.; Abetz, V.; Krausch, G. *Macromolecules* **2002**, *35*, 5570.
(62) Breiner, U.; Krappe, U.; Abetz, V.; Stadler, R. *Macromol. Chem. Phys.* **1997**, *198*, 1051.

MA049048D